

Article

# Poly (O-Aminophenol) Produced by Plasma Polymerization Has IR Spectrum Consistent with a Mixture of Quinoid & Keto Structures

Natalie M. Stuart<sup>1</sup> and Karl Sohlberg<sup>1,2,\*</sup> <sup>1</sup> Department of Chemistry, Drexel University, Philadelphia, PA 19104, USA; nms347@drexel.edu<sup>2</sup> Department of Materials Science & Engineering, Drexel University, Philadelphia, PA 19104, USA

\* Correspondence: kws24@drexel.edu

**Abstract:** A vibrational analysis of various poly(o-aminophenol) structures has been undertaken using first principles methods. It is shown that a mixture of quinoid and keto forms of poly(o-aminophenol) gives rise to a simulated spectrum that replicates the experimental infrared spectra of plasma-produced poly(o-aminophenol) better than either the quinoid or keto poly(o-aminophenol) spectra alone. An unassigned peak in the spectrum is attributed to hydrogen bonding to the silica substrate.

**Keywords:** poly(o-aminophenol); IR spectrum; vibrational frequencies; theoretical calculations; dielectric barrier discharge plasma



**Citation:** Stuart, N.M.; Sohlberg, K. Poly (O-Aminophenol) Produced by Plasma Polymerization Has IR Spectrum Consistent with a Mixture of Quinoid & Keto Structures. *Plasma* **2022**, *5*, 196–205. <https://doi.org/10.3390/plasma5020015>

Academic Editor:  
Andrey Starikovskiy

Received: 25 January 2022

Accepted: 11 April 2022

Published: 14 April 2022

**Publisher's Note:** MDPI stays neutral with regard to jurisdictional claims in published maps and institutional affiliations.



**Copyright:** © 2022 by the authors. Licensee MDPI, Basel, Switzerland. This article is an open access article distributed under the terms and conditions of the Creative Commons Attribution (CC BY) license (<https://creativecommons.org/licenses/by/4.0/>).

## 1. Introduction

Conductive polymers, such as polyaniline (PAN) and its derivatives, are widely studied due to their promising electric and optical properties, tunable configurations, and relatively low cost. PAN is commonly utilized in energy storage devices, such as rechargeable batteries, and chemical sensor applications [1,2]. Aminophenols are derivatives of anilines that benefit from containing two reaction points, amino (-NH<sub>2</sub>) and hydroxyl (-OH) groups, that can be oxidized. Thus, aminophenols yield electrochemical properties comparable to those of both anilines and phenols [3]. Specifically, poly(o-aminophenol) (PoAP) finds use in solar cell technologies [4] and as a chemical sensor for glucose [5,6] and uric acid [7]. It has recently been demonstrated by Chen et al. [8] that PoAP can be easily synthesized by exposing the ortho-aminophenol (oAP) monomer to dielectric barrier discharge (DBD) plasma. Their process produces polymerized o-aminophenol, as confirmed by Fourier Transform Infrared (FTIR) and ultraviolet-visible (UV-Vis) spectroscopy [8].

It is commonly known that the structure of PoAP can exhibit a ladder-like or open-chain form [9]. Upon oxidation, the quinoid [10] and keto [11,12] forms are the predominant structures of PoAP. These non-oxidated and oxidated structures are all represented in Figure 1.

Plasma treatment is an oxidative process, and thus it is reasonable to deduce that DBD plasma-produced PoAP would not feature un-oxidized ladder-like and open-chain structures (See Figure 1), as is the conclusion of Chen et al. [8]. The researchers identified their PoAP as having a quinoid structure, based on FTIR spectra featuring C=O stretching, C–O–C stretching, C=N stretching, and C–N stretching, while lacking N–H and O–H stretching frequencies. Plasma treatment is also commonly understood to be a highly reactive process, however, due to the ionized nature of the plasma gas. In concert with aminophenol's reactive amino and hydroxyl groups, we propose that DBD plasma-produced PoAP may exhibit both oxidized quinoid and keto structures. It is not uncommon for more than one polymeric structure to be formed due to the multiple reaction points on the monomer. The works of Al-Hossainy et al. [4] and Bicak et al. [5] both report synthesizing PoAP structures containing both quinoid and benzoid rings after oxidation via ferric chloride/hydrochloric acid and copper bromide, respectively. As previously mentioned, it is reasonable to conclude that the PoAP product synthesized by Chen et al. [8] would

feature oxidized structures, though the relative abundance of the quinoid and keto forms (See Figure 1) remains unresolved. In this paper, we report the application of theoretical modeling of the infrared (IR) spectra of PoAP to explore the relative abundance of the quinoid and keto forms.

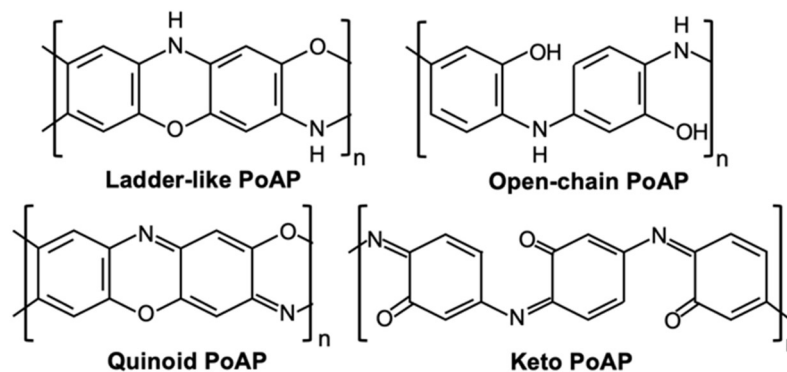


**Figure 1.** Non-oxidated (ladder-like and open-chain) and oxidated (quinoid and keto) structures of PoAP.

## 2. Materials and Methods

Electronic structure calculations and geometric optimization by energy minimization were carried out on the monomer and oligomers of oAP using density functional theory (DFT) with the hybrid B3LYP [13,14] functional at the 6-31G(d) [15,16] level of theory using the General Atomic and Molecular Electronic Structure System (GAMESS) suite of codes [17]. The threshold for geometric convergence was taken to be 0.0001 Hartree/Bohr. The optimized geometries were subsequently subjected to analytic Hessian calculations. All vibrational frequencies were scaled by a factor of 0.9614, which has been recommended by Scott and Radom [18] as optimal for the DFT/B3LYP/6-31G(d) level of theory. The vibrational modes were visualized & animated using Facio graphical user interface (GUI) software [19], to identify those modes corresponding to each prominent functional group (C=O, C=N stretching, etc.). The GUI was also used to generate theoretically predicted spectra from (frequency, intensity) data obtained from the electronic structure calculations. The experimental IR spectrum of Chen et al. [8], as well as the spectra predicted with the Facio [19] software, were digitized using WebPlotDigitizer [20] to facilitate a comparison.

### 2.1. Procedure

First, monomer structures for quinoid and keto o-aminophenol were optimized. From these optimized monomers, initial structural models of quinoid and keto trimers, (taken here to be representative of the full polymer) were constructed and subjected to structural optimization. Fully optimized structures for quinoid and keto trimers are shown in Figure 2A,B, respectively. Subsequently, harmonic normal mode vibrational frequencies were computed. Earlier computational work on oligomers of 3-phenyl-1-ureidonitrile [21] showed C=N stretching frequencies to be well converged with respect to the degree of oligomerization in the trimer, supporting the choice of trimer to represent the full polymer. Convergence tests on the present keto and quinoid o-aminophenol systems confirmed this choice. It was found that peak intensities for the dominant peaks used in the fitting are well converged at the trimer, with a mean unsigned difference between the trimer and tetramer intensities of 12%.

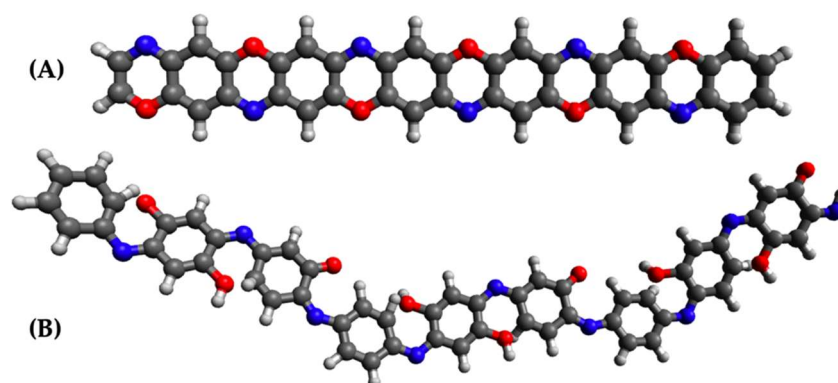


**Figure 2.** Trimer (A) quinoid and (B) keto oAP molecular structures, which were subjected to optimization by energy minimization at the DFT/B3LYP/6-31G(d) level of theory. Structures were visualized with Avogadro [22] GUI software.

Once predicted vibrational frequencies were obtained for the quinoid and keto PoAP trimer structures, which are shown in Figure 3B,C, respectively, a GUI software [19] was used to animate each vibrational mode. Thus, the C=O stretching, C=N stretching, C=C stretching, C–N stretching of aromatic rings, and C–O–C stretching modes were identified by visual inspection. A simulated spectrum for the polymer, shown in Figure 3D, was generated by finding the weighted average of the predicted quinoid and keto spectra that produces intensities for the dominant peaks in the best agreement with the experimental spectrum of Chen et al. [8]. This procedure consists of two steps: digitizing and optimization.

#### 2.1.1. Digitizing

First, the experimental PoAP spectra of Chen et al. [8] were reconstructed based on a digitization of the published spectrum, as shown in Figure 3A. This was done by uploading an image of the published spectrum to WebPlotDigitizer [20] and collecting an intensity data point at each wavenumber from 500–3500  $\text{cm}^{-1}$ . The major peaks were identified as those ca.  $\nu = 1639, 1601, 1461, 1281, 1230, 1110,$  and  $1050 \text{ cm}^{-1}$  in the experimental spectrum. All spectral intensities were converted from percent transmittance to absorbance to facilitate intensity comparisons. The theoretical keto and quinoid trimer spectra were also digitized to facilitate a direct comparison between the theoretical intensities and the experimental PoAP spectral intensities.

#### 2.1.2. Optimization

Next, a linear combination of theoretical intensities was generated to find the best match to the experimental spectrum. A simulated spectrum was produced by taking a weighted average of the theoretical intensity  $I_{\text{theo}(\nu)}^{\text{quinoid}}$  and  $I_{\text{theo}(\nu)}^{\text{keto}}$  values. By conservation of mass, the weights on the quinoid and keto forms must sum to 1, and thus, the weighted average of the theoretical intensities can be rewritten as:

$$I_{\text{sim}(\nu)} = c \left( A * I_{\text{theo}(\nu)}^{\text{quinoid}} \right) + (1 - c) \left( A * I_{\text{theo}(\nu)}^{\text{keto}} \right) \quad (1)$$

in which  $A$  is a normalization factor applied to all theoretical frequencies to facilitate comparison with the experimental intensities. The relative abundances of the quinoid and keto forms are represented by  $c$  and  $(1 - c)$ , respectively. The optimal weighting factor  $c$  was determined by minimizing the sum of squares of differences ( $\varepsilon$ ) between the  $I_{\text{sim}(\nu)}$  and experimental  $I_{\text{exp}(\nu)}$  intensities:

$$\varepsilon = \sum_{\nu} \left( I_{\text{sim}(\nu)} - I_{\text{theo}(\nu)} \right)^2 \quad (2)$$

by varying factors  $c$  and  $A$ . Here, the sum runs over the three most prominent composite peaks ( $\nu = 1605, 1406, \text{ and } 1179 \text{ cm}^{-1}$ ) and their experimental counterparts ( $\nu = 1601, 1461, \text{ and } 1281 \text{ cm}^{-1}$ ), respectively.

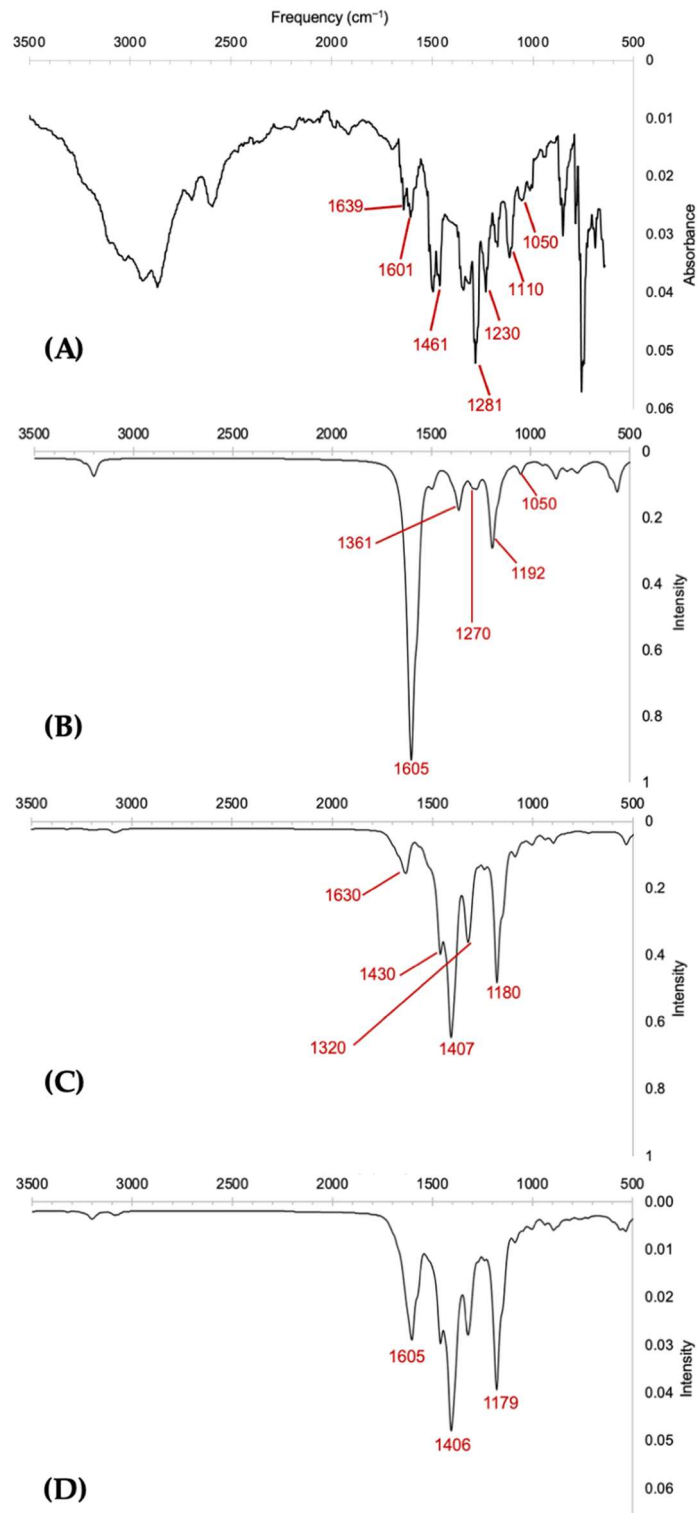


**Figure 3.** (A) Experimental spectra of PoAP (after DBD plasma treatment) obtained via attenuated total reflection [8]. (B) Theoretical spectra for quinoid PoAP trimer. (C) Theoretical spectra for keto PoAP trimer. (D) Simulated spectra comprised of 27% quinoid and 73% keto PoAP structures.

### 3. Results and Discussion

Vibrational assignments for the major peaks in the experimental spectrum of DBD-plasma-produced PoAP are collected in Table 1 together with the corresponding theoretically computed frequencies for the quinoid and keto trimers and analogous experimental values from the literature. The theoretical frequencies are in reasonable quantitative agreement with those reported by Chen et al. [8] and with the literature values. Though the quinoid spectra do reproduce some of the major peaks seen in the experimental spectrum, the intensities of the peaks are not consistent with the experiment. The DBD plasma-produced PoAP spectrum exhibits the most intense peak at  $1281\text{ cm}^{-1}$ , corresponding to C–N stretching of aromatic rings [8]. The theoretical quinoid spectrum exhibits an absorbance at  $1289\text{ cm}^{-1}$ , but its intensity (relative to the other peaks in the theoretical spectrum) is much lower than that seen in the experimental spectrum. The theoretical keto structure, however, does exhibit an intense peak at  $1298\text{ cm}^{-1}$ . Because the keto structure exhibits a C–N aromatic ring stretching peak that is more consistent with the experimental data, it is reasonable to postulate that a linear combination of quinoid and keto frequencies could produce a simulated spectrum in better agreement with the experimental data than the quinoid spectra alone.

**Table 1.** Major peak descriptions for DBD plasma-produced PoAP, theoretical & literature values for quinoid and keto PoAP.

Vibration Assignments	Wavenumber, $\text{cm}^{-1}$				
	Chen et al. [8]	Theo. Quinoid	Theo. Keto	Lit. Quinoid	Lit. Keto
C=O stretching	n/a	n/a	1669, 1697	n/a	1670–1690 [23]
C=N stretching	1639	1613, 1615, 1622, 1636	1620, 1625, 1637	1645 [23]	n/a
C=C stretching	1461, 1601	1397, 1491, 1572, 1595, 1600, 1605	1378, 1392, 1403, 1411, 1431, 1455, 1563	1430–1613 [9,23]	1450, 1590 [5,23]
C–N stretching of aromatic ring	1281	1289, 1297	1170, 1298, 1300, 1307	1284 [9]	n/a
C–O–C stretching	1050, 1110, 1230	1049, 1161, 1193, 1270	1036, 1047, 1072, 1078, 1082, 1237	1050, 1112 [5] 1235 [23]	1050, 1235 [23]

#### 3.1. Simulated Spectrum

The predicted spectra for quinoid and keto trimers are shown in Figure 3B,C, respectively. It was found that  $c = 0.27$  generated the lowest sum-of-squares of differences expressed in Equation (3), suggesting that the experimental spectrum represented a mixture of 27% quinoid and 73% keto PoAP. The simulated spectrum is shown in Figure 3D. The intensities of the peaks in the simulated spectrum arising from a mixture of forms are qualitatively a better match to the experimental spectrum than either the quinoid or keto spectra alone.

#### 3.2. Packing Efficiency

One factor that introduces some uncertainty into the estimated composition is the packing efficiency. The theoretical intensities may be assumed to be proportional to the absorbance of a single molecule, but because the monomers differ in size, one can reasonably expect a higher number density of the smaller species in a physical sample. Two approaches to estimating this factor produce nearly identical results. The first approach is to compare molecular volumes [24]. The keto monomer has an estimated volume of  $V_k = 270\text{ \AA}^3$  and the quinoid monomer an estimated volume of  $V_q = 198\text{ \AA}^3$ . Within a fixed sample volume ( $V$ ), the ratio of number densities is  $\frac{n_q/V}{n_k/V} = \frac{V_k}{V_q} = 1.36$ . The second approach starts by assuming that the two forms of the polymer have the same density. (This approximation

is consistent with the observation that many organic polymers have very similar material densities, typically in the range of [0.9–1.0] g/cc.) Given that density is mass per unit volume, equating densities written in terms of molecular weight ( $M$ ) and molar quantity ( $n$ ) gives,  $\frac{n_k M_k}{V} = \frac{n_q M_q}{V}$ , which may be rearranged into,  $\frac{n_q}{n_k} = \frac{M_k}{M_q} = \frac{317}{236} = 1.34$ .

To investigate the possible effect of packing efficiency on the peak fitting analysis, a composite spectrum was generated from a linear combination of keto and quinoid intensities, in which the quinoid intensities were multiplied by the factor 1.34 before optimization of the fitting parameters. Equation (1), when modified to include this concentration factor, may be written as:

$$I_{\text{sim}(\nu)} = c \left( A * 1.34 * I_{\text{theo}(\nu)}^{\text{quinoid}} \right) + (1 - c) \left( A * I_{\text{theo}(\nu)}^{\text{keto}} \right) \quad (3)$$

Optimizing the  $c$  and  $A$  factors in Equation (3) to minimize the sum-of-squares of difference as expressed in Equation (3) produced  $c = 0.21$ . Thus, after applying the packing efficiency factor to the theoretical quinoid intensities, the experimental spectrum can be represented by a composite spectrum of 21% quinoid and 79% keto structures. This result is 6% different than the composite spectrum generated without the packing efficiency factor, which is one possible estimate of the uncertainty in the peak fitting analysis.

### 3.3. Unidentified Peak

One feature in the experimental spectrum of PoAP that is not captured by the simulated spectrum is the broad peak in the range of 2600–3300  $\text{cm}^{-1}$ . The work of Chen et al. [8] did not report an assignment for this peak, as it was not featured in their polymerization identification process. It should also be noted that this broad peak is seen in their FTIR spectra for the monomer oAP as well as PoAP, indicating that it does not arise from a structure created by polymerization [8].

To create the most accurate linear combination of quinoid and keto structures, several attempts were made to identify the origin of this broad peak and remove it (and other associated contaminant peaks) from the experimental spectra. While C–H stretching is known to produce absorbance in the  $\sim 3000 \text{ cm}^{-1}$  region, the broad peak was not reproduced by the vibrational frequency calculations for either the quinoid or keto structure, nor does it appear in the computed spectra of the monomer (not shown here). The work of Bicak et al. also described a broad peak at  $\sim 3200 \text{ cm}^{-1}$  in their FTIR spectroscopic studies of PoAP, reportedly due to the hydroxyl stretching of free –OH groups, the presence of which they confirmed by proton NMR [5]. Thus, the first possible assignment considered for the broad peak was hydroxyl stretching from the ethanol solvent used in the experiment of Chen et al. [8]. The removal of the hypothesized ethanol absorbance from the experimental spectrum to create a new simulated spectrum consisted of three steps: digitization, subtraction, and optimization.

First, an FTIR spectrum of ethanol was obtained from the National Institute of Standards and Technology (NIST) [25] and digitized (Figure 4), as described in the Procedure section. For consistency, an ethanol spectrum having the same resolution ( $4 \text{ cm}^{-1}$ ) as the experimental spectra of Chen et al. [8] was selected. Since the intensities of the ethanol peaks were not on the same scale as those in the experimental PoAP spectrum, the ethanol spectrum had to be normalized to facilitate an intensity comparison. This was done by identifying the most intense ethanol peak ( $\nu = 2974 \text{ cm}^{-1}$ ,  $A = 1.92$ ) and calculating a scaling factor ( $S$ ) (See Equation (4)) such that this peak would be of equal intensity to the (assumed corresponding) peak at  $2974 \text{ cm}^{-1}$  in Chen et al.'s spectrum of PoAP ( $S = 0.01859$ ).

$$S = \frac{A_{\text{PoAP}(\nu)}}{A_{\text{ethanol}(\nu)}} \quad (4)$$

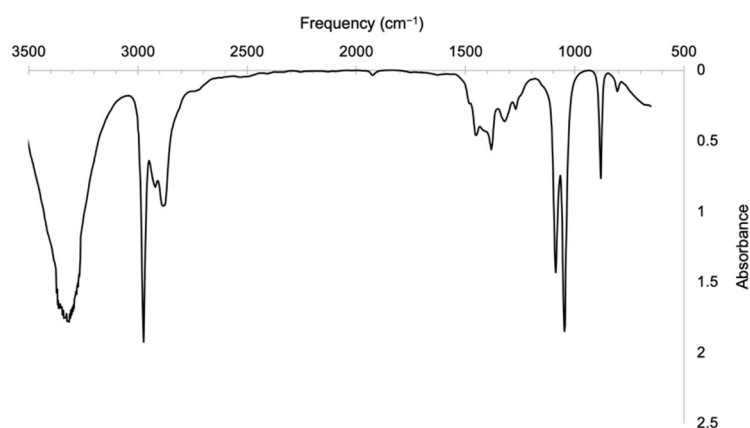


**Figure 4.** Experimental spectra of ethanol obtained from NIST database [25].

The ethanol absorbances were all multiplied by this scaling factor  $S$ , generating a normalized ethanol spectrum. The normalized ethanol intensities at each wavenumber from 500–3500  $\text{cm}^{-1}$  were then subtracted from those of the experimental PoAP spectrum, generating a “decontaminated” experimental PoAP spectrum with the (assumed) contribution from ethanol removed.

After the decontaminated experimental PoAP spectrum with intensities  $I_{\text{exp}(\nu)}^{\text{scaled}}$  was generated, the peak fitting analysis was completed as described in the Procedure section. Equation (2) was utilized to generate a weighted sum of the quinoid and keto spectra that would best reproduce the intensities at 1601, 1461, and 1281  $\text{cm}^{-1}$  in the decontaminated experimental spectrum. The substitution of Equation (1) into Equation (2) and optimization of the  $A$  and  $c$  parameters in the resulting expression found that  $c = 0.30$  minimized the sum-of-squares of difference between  $I_{\text{sim}(\nu)}$  and  $I_{\text{exp}(\nu)}^{\text{scaled}}$ , suggesting that the scaled experimental spectrum with ethanol removed can be represented by a composite spectrum featuring 30% quinoid and 70% keto forms. This change in  $c$  of 3% from the original fitting is smaller in magnitude than the change introduced by estimating the effect of the packing efficiency. Therefore, it is reasonable to conclude that removal of ethanol contributions does not change the predicted percentages of quinoid and keto structures at a significant level.

Further analysis suggests that there are several additional reasons to conclude that ethanol is unlikely to be responsible for the unidentified peak. First, ethanol exhibits a strong, sharp absorbance of  $\sim 1050 \text{ cm}^{-1}$ , which does not appear in the spectrum of the polymer. Consequently, after subtraction of the (postulated) contribution from ethanol, the experimental spectrum exhibits a strong negative absorbance, which is unphysical. Second, the OH stretching band of ethanol is not well matched in shape or position to the broad unidentified peak in the experimental spectrum of the polymer. Third, ethanol would most likely be vaporized upon plasma treatment and thus would not be visible in the experimental spectra.

Another possible explanation for the broad unidentified peak is based on the observation that the shape of the broad peak is reminiscent of those resulting from the hydroxyl stretching of carboxylic acid dimers, which produces strong and broad peaks in the 2300–3300  $\text{cm}^{-1}$  region [26]. Carboxylic acids form dimers through hydrogen bonding, which effectively red-shifts the O–H stretching adsorption compared to that of the monomer [27,28]. Although there is no obvious source of carboxylic acids in the polymer sample, red-shifted O–H stretching vibrations could arise from H-bonding interactions between the polymer (or monomer) and the  $\text{SiO}_2$  surface, which was used as a support in the experimental synthesis of plasma-produced PoAP [8].

To explore this possibility, calculations were carried out to investigate the behavior of the O–H stretching frequency when the –OH moiety was engaged in hydrogen bonding to the silicon oxide surface. A cluster model of aminophenol hydrogen-bonded to a silica-containing species is shown schematically in Figure 5.

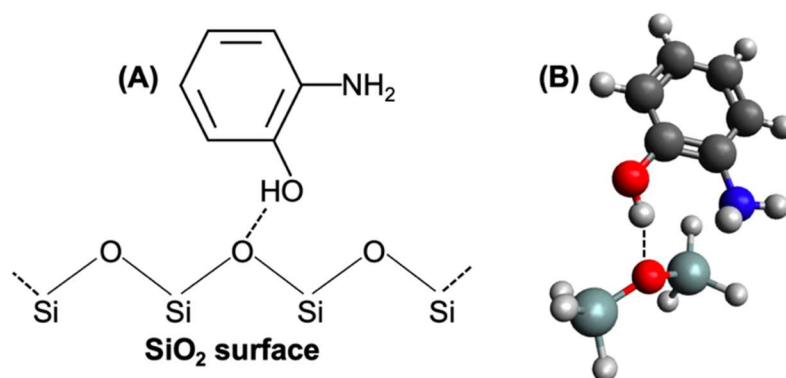


**Figure 5.** (A) Schematic representation of o-aminophenol H-binding to a SiO<sub>2</sub> surface. (B) A molecular model of aminophenol binding to disiloxane was simulated for this analysis. In (B), dark grey, light grey, red, dark blue, and teal circles represent carbon, hydrogen, oxygen, nitrogen, and silicon atoms, respectively.

This influence of the interaction between aminophenol and silica was simulated by calculating the vibrational frequencies for an aminophenol molecule and determining its O–H stretching frequency, then adding a disiloxane molecule near the aminophenol’s hydroxyl group and re-calculating the aminophenol’s O–H stretching absorption.

First, a model of an o-aminophenol monomer was fully optimized, and the energy second derivatives were calculated to find its vibrational frequencies. A GUI software [19] was used to animate each vibrational mode, and the scaled [18] DFT/B3LYP/6-31G(d) frequency corresponding to O–H stretching was found to be 3862 cm<sup>−1</sup> with an intensity of 3.6 (arb. units). The o-aminophenol monomer was then re-optimized with a disiloxane molecule in close proximity. The disiloxane molecule was oriented such that its oxygen atom was adjacent to the hydrogen on the oAP’s OH functional group and the amino group was out of plane from the disiloxane’s oxygen to attenuate potential hydrogen bonding between the oAP amino group and the disiloxane oxygen. The vibrational frequencies of the oAP and disiloxane molecule were calculated. An empirical dispersion correction [29] was specified to model hydrogen-bonding. The scaled O–H stretching frequency of AP–OH–silanol was found to be 3413 cm<sup>−1</sup> with an intensity of 16.

The change in  $\nu_{\text{OH}}$  with the addition of disiloxane was  $-449 \text{ cm}^{-1}$ , paired with a fourfold increase in intensity. Clearly, H-bonding to the heavy silicon atom effectively decreases/red-shifts the vibrational frequency of O–H stretching. Additionally, the increase in intensity with proximity to Si atoms would explain the relative strength of the broad unidentified peak in the experimental spectrum of Chen et al. [8]. These results can be extrapolated to suggest that the plasma-produced PoAP is exhibiting H-bonding with the SiO<sub>2</sub> surface, effectively causing its O-H stretching modes to absorb strongly in the 2600–3300 cm<sup>−1</sup> range. It seems most reasonable to conclude that the broad unidentified peak arises from H-bonding interactions with the SiO<sub>2</sub> substrate. Under that assumption, no contaminant subtraction is necessary. Regardless, the predicted quinoid:keto ratio is ca. 27:73.

#### 4. Conclusions

Optimized geometries of quinoid and keto PoAP trimers (taken to be representative of the polymer) were obtained using first principles methods. Harmonic vibrational frequencies were then calculated using analytic second derivatives. A least-squares fitting was used to find the weighting factors for the two forms that produced a simulated spectrum in best agreement with the experiment. It corresponds to 27% quinoid and 73% keto PoAP and is qualitatively more similar to the experimental spectrum of DBD plasma-produced PoAP than the spectra of either quinoid or keto structures alone. A second simulated spectrum was created after subtracting a (supposed) contribution of ethanol from the experimental spectra, but the experimental spectrum after subtraction exhibited a

strong unphysical negative absorbance. This observation, coupled with the likely loss of ethanol during plasma treatment, leads us to dismiss ethanol as an appreciable contributor to the experimental spectrum. The vibrational analysis of the shift in OH stretching upon hydrogen bonding and literature reports of the shape of IR peaks corresponding to hydrogen-bond-shifted OH vibrations suggest that the most probable origin of a broad unidentified peak in the experimental spectrum of both the polymer and its unpolymerized monomer is the red-shifting of OH vibrations due to H-bonding interactions with the SiO<sub>2</sub> substrate.

Overall, the present vibrational frequency analysis reveals that the IR spectrum of poly(o-aminophenol) produced by DBD plasma treatment can be more accurately described by the presence of quinoid and keto structures than by the quinoid structure alone.

**Author Contributions:** Conceptualization, N.M.S. and K.S.; methodology, N.M.S.; software, N.M.S. and K.S.; validation, N.M.S. and K.S.; investigation, N.M.S.; resources, K.S.; data curation, N.M.S.; writing—original draft preparation, N.M.S.; writing—review and editing, K.S. and N.M.S.; visualization, N.M.S.; supervision, K.S.; project administration, K.S.; funding acquisition, K.S. All authors have read and agreed to the published version of the manuscript.

**Funding:** This research was funded in part by ACS PRF #58323-ND10, for which the KS group thanks the donors of the American Chemical Society Petroleum Research Fund.

**Acknowledgments:** The authors thank H.-F. Ji for discussions of the experimental IR spectrum, and B. Rosen for computer hardware and software maintenance.

**Conflicts of Interest:** The authors declare no conflict of interest.

## References

1. Manisankar, P.; Vedhi, C.; Selvanathan, G.; Somasundaram, R. Electrochemical and electrochromic behavior of novel poly (aniline-co-4, 4'-diaminodiphenyl Sulfone). *Chem. Mater.* **2005**, *17*, 1722–1727. [[CrossRef](#)]
2. Karami, H.; Mousavi, M.F.; Shamsipur, M. A new design for dry polyaniline rechargeable batteries. *J. Power Sources* **2003**, *117*, 255–259. [[CrossRef](#)]
3. Gopalasamy, T.; Gopalswamy, M.; Gopichand, M.; Raj, J. Poly Meta-Aminophenol: Chemical synthesis, characterization and AC impedance study. *J. Polym.* **2014**, *2014*, 27043. [[CrossRef](#)]
4. Al-Hossainy, A.; Zoromba, M.S.; Abdel-Aziz, M.; Bassyouni, M.; Attar, A.; Zwawi, M.; Abd-Elmageed, A.; Maddah, H.; Slimane, A.B. Fabrication of heterojunction diode using doped-poly (ortho-aminophenol) for solar cells applications. *Phys. B Condens. Matter* **2019**, *566*, 6–16. [[CrossRef](#)]
5. Bicak, T.C.; Soylemez, S.; Buber, E.; Toppare, L.; Yagci, Y. Poly (o-aminophenol) prepared by Cu (II) catalyzed air oxidation and its use as a bio-sensing architecture. *Polym. Chem.* **2017**, *8*, 3881–3888. [[CrossRef](#)]
6. Pan, D.; Chen, J.; Yao, S.; Tao, W.; Nie, L. An amperometric glucose biosensor based on glucose oxidase immobilized in electropolymerized poly (o-aminophenol) and carbon nanotubes composite film on a gold electrode. *Anal. Sci.* **2005**, *21*, 367–371. [[CrossRef](#)]
7. Miland, E.; Ordieres, A.M.; Blanco, P.T.; Smyth, M.; Fagain, C. Poly (o-aminophenol)-modified bienzyme carbon paste electrode for the detection of uric acid. *Talanta* **1996**, *43*, 785–796. [[CrossRef](#)]
8. Chen, K.; Cao, M.; Feng, E.; Sohlberg, K.; Ji, H.-F. Polymerization of Solid-State Aminophenol to Polyaniline Derivative Using a Dielectric Barrier Discharge Plasma. *Plasma* **2020**, *3*, 187–195. [[CrossRef](#)]
9. Ghanem, M.A.; El-Enany, G. Development of conducting poly (o-aminophenol) film and its capacitance behavior. *Int. J. Electrochem. Sci.* **2016**, *11*, 9987–9997. [[CrossRef](#)]
10. Ohsaka, T.; Watanabe, T.; Kitamura, F.; Oyama, N.; Tokuda, K. Electrocatalysis of O<sub>2</sub> reduction at poly (o-phenylenediamine)-and poly (o-aminophenol)-coated glassy carbon electrodes. *J. Chem. Soc. Chem. Commun.* **1991**, *16*, 1072–1073. [[CrossRef](#)]
11. Zhang, A.; Cui, C.; Chen, Y.; Lee, J. Synthesis and electrochromic properties of poly-o-aminophenol. *J. Electroanal. Chem.* **1994**, *373*, 115–121. [[CrossRef](#)]
12. Tucceri, I.R. Poly (o-aminophenol) as material of biosensors. *Res. Open Access* **2014**, *2014*, 884. [[CrossRef](#)]
13. Becke, A.D. Density-functional exchange-energy approximation with correct asymptotic behavior. *Phys. Rev. A* **1988**, *38*, 3098. [[CrossRef](#)] [[PubMed](#)]
14. Lee, C.; Yang, W.; Parr, R.G. Development of the Colle-Salvetti correlation-energy formula into a functional of the electron density. *Phys. Rev. B* **1988**, *37*, 785–789. [[CrossRef](#)]
15. Hehre, W.J.; Ditchfield, R.; Pople, J.A. Self-Consistent molecular orbital methods. XII. Further extensions of Gaussian—Type basis sets for use in molecular orbital studies of organic molecules. *J. Chem. Phys.* **1972**, *56*, 2257–2261. [[CrossRef](#)]

16. Hariharan, P.C.; Pople, J.A. The influence of polarization functions on molecular orbital hydrogenation energies. *Theor. Chim. Acta* **1973**, *28*, 213–222. [[CrossRef](#)]
17. Barca, G.M.J.; Bertoni, C.; Carrington, L.; Datta, D.; De Silva, N.; Deustua, J.E.; Fedorov, D.G.; Gour, J.R.; Gunina, A.O.; Guidez, E.; et al. Recent developments in the general atomic and molecular electronic structure system. *J. Chem. Phys.* **2020**, *152*, 154102. [[CrossRef](#)]
18. Scott, A.P.; Radom, L. Harmonic vibrational frequencies: An evaluation of Hartree–Fock, Møller–Plesset, quadratic configuration interaction, density functional theory, and semiempirical scale factors. *J. Phys. Chem.* **1996**, *100*, 16502–16513. [[CrossRef](#)]
19. Suenaga, M. Facio. Available online: <http://zzzfelis.sakura.ne.jp/index.html> (accessed on 10 March 2021).
20. Rohatgi, A. WebPlotDigitizer. Available online: <https://automeris.io/WebPlotDigitizer> (accessed on 18 October 2021).
21. Silver, A.; Dong, H.; Sun, Z.; Sohlberg, K. Semiempirical study of low molecular weight polymers of 3-phenyl-1-ureidonitrile. *J. Mol. Struct. THEOCHEM* **2005**, *731*, 149–155. [[CrossRef](#)]
22. Avogadro: An Open-Source Molecular Builder and Visualization Tool; Version 1.2.0; Available online: <http://avogadro.cc/> (accessed on 18 October 2021).
23. Kunimura, S.; Ohsaka, T.; Oyama, N. Preparation of thin polymeric films on electrode surfaces by electropolymerization of o-aminophenol. *Macromolecules* **1988**, *21*, 894–900. [[CrossRef](#)]
24. Molinspiration Chemoinformatic Software. Available online: <https://www.molinspiration.com> (accessed on 10 February 2022).
25. Smith, A.L. *The Coblentz Society Desk Book of Infrared Spectra*, 2nd ed.; Coblentz Society: Kirkwood, MO, USA, 1982; pp. 1–24.
26. James, C.; Ravikumar, C.; Sundius, T.; Krishnakumar, V.; Kesavamoorthy, R.; Jayakumar, V.; Joe, I.H. FT-Raman and FTIR spectra, normal coordinate analysis and ab initio computations of (2-methylphenoxy) acetic acid dimer. *Vib. Spectrosc.* **2008**, *47*, 10–20. [[CrossRef](#)]
27. Shipman, S.T.; Douglass, P.C.; Yoo, H.S.; Hinkle, C.E.; Mierzejewski, E.L.; Pate, B.H. Vibrational dynamics of carboxylic acid dimers in gas and dilute solution. *Phys. Chem. Chem. Phys.* **2007**, *9*, 4572–4586. [[CrossRef](#)] [[PubMed](#)]
28. Dubis, A.T.; Grabowski, S.J.; Romanowska, D.B.; Misiaszek, T.; Leszczynski, J. Pyrrole-2-carboxylic acid and its dimers: Molecular structures and vibrational spectrum. *J. Phys. Chem. A* **2002**, *106*, 10613–10621. [[CrossRef](#)]
29. Grimme, S. Accurate description of van der Waals complexes by density functional theory including empirical corrections. *J. Comput. Chem.* **2004**, *25*, 1463–1473. [[CrossRef](#)]